AAS 13-836

QUATERNION BASED OPTIMAL SPACECRAFT REORIENTATION UNDER COMPLEX ATTITUDE CONSTRAINED ZONES

Unsik Lee* **and Mehran Mesbahi†**

The paper addresses quaternion-based energy and time optimal spacecraft reorientation in the presence of complex attitude constrained zones. Designing an optimal reorientation trajectory for a rigid body spacecraft is posed as a nonlinear optimal control problem. In this direction, attitude constrained zones are defined with respect to the onboard instrument under two categories, forbidden and mandatory zones. These zones are parameterized as quadratic inequality constraints in unit quaternions. The optimal control problem is then solved using a Gauss pseudospectral method. Ambiguity on geodesic/non-geodesic rotations which is a consequence of the quaternion formulation, is discussed and a novel algorithm is presented for its treatment. The paper concludes with extensive simulation results including typical scenarios many science mission spacecraft face as well as more complex scenarios in order to demonstrate the viability of the proposed methodology.

INTRODUCTION

One of the key technologies of modern small spacecraft is fine attitude control, requiring high pointing accuracy and regulation.[2] As space system technology has developed, smaller spacecraft, in the category of microsatellites, have emerged as new candidates for space science missions. Recently developed micro reaction wheels enable microsatellites to execute large angle reorientations. Planning a reorientation, while avoiding undesirable orientations with respect to celestial objects is essential for science missions. For example, microsatellites equipped with sensitive payloads, such as infrared telescopes or interferometers, require re-targeting while keeping away from direct exposure to the sunlight or other bright objects. In order to conduct such missions with limited resources, energy/time optimal control assumes a critical role.

The spacecraft reorientation problem in the absence of attitude constrained zones has been comprehensively addressed in nonlinear control literature[19,20] using techniques such as backstepping[13,14] and sliding mode control.[3] Particularly in the optimal control framework, both indirect[4,5] and direct methods[7] often use rotation matrix parameterization of attitude over the unit quaternion formulation. The choice of the rotation matrix, even though it requires more parameters to process than the unit quaternions, is due to the fact that unit quaternions doubly cover $\mathsf{SO}(3)$. This fact often leads the spacecraft to traverse a longer non-geodesic as opposed to a geodesic rotation. For optimal reorientations, the treatment of geodesic/non-geodesic rotations is important issue since non-geodesic rotations require extra time and energy for executing the reorientation.

In the meantime, the attitude reorientation problem in the presence of attitude constrained zones has been examined in a limited number of research works. For example, McInnes considered and

*Graduate Student, W. E. Boeing of Dept. of Aero & Astronautics, University of Washington, Seattle, WA 98195.
†Professor, W. E. Boeing of Dept. of Aero & Astronautics, University of Washington, Seattle, WA 98195.

implemented maneuver planning in the presence of attitude constrained zones via an artificial potential function.[1] However, due to the use of Euler angles in McInnes' works, the possibility of having performance degrading singularities during reorientation maneuvers could not be eliminated. Another set of approaches to constrained attitude control which rely on geometric relations between the direction of an instrument's boresight and a bright celestial object to be avoided, has been introduced by Spindler[8] and Hablani.[9] In these research works, a feasible attitude trajectory is determined prior to the reorientation maneuver and generated based on the geometric formulation of the exclusion zones. These approaches have a weakness of not being extendible to more complex situations, involving multiple celestial constrained zones, as often encountered in actual space missions.

Over the last decade, alternative approaches using randomized algorithms have also been proposed by Frazzoli *et al.*,[10] Kornfeld,[11] and Cui *et al.*[12] The randomization-based approaches have an advantage in terms of their ability to handle distinct classes of constraints, with provable–albeit probabilistic–convergence properties. The randomized algorithms, however, have limitations in terms of their on-board implementation and may result in execution times that, depending on the types of constrained zones and initial and final attitudes, can be of exponential order.

In this paper, we expand on our earlier results on attitude constrained zone parameterization[6] and propose a novel algorithm which addresses the geodesic/non-geodesic rotation problem. We present an approach for optimal attitude path planning in the presence of attitude constrained zones that uses minimal energy and time. The problem is solved via Gauss pseudospectral method where the optimal control problem is discretized at collocation points, and then transcribed to a nonlinear programming problem (NLP).

UNIT QUATERNIONS AND GEODISIC ROTATION

The attitude of a rigid spacecraft, describing its relative orientation between a reference frame and the body fixed frame, evolves on the special orthogonal group of order three $\mathsf{SO}(3)$. Formally,

$$\mathsf{SO}(3) = \{\, R \in \mathbf{R}^{3\times 3} \mid R^T R = I_3 \text{ and } \det(R) = 1 \,\}, \tag{1}$$

where I_3 is a identity matrix in R^3. Unit quaternions, elements of the three dimensional unit sphere S^3, are popularly used to parameterize $\mathsf{SO}(3)$. The corresponding configuration space is a boundaryless compact manifold, defined by

$$S^3 = \{\, \mathbf{q} \in \mathbf{R}^4 \mid \|\, \mathbf{q} \,\| = 1 \,\}, \tag{2}$$

where $\mathbf{q} = [\, \boldsymbol{q}^T \;\; q_0 \,]^T \in S^3$. Unit quaternions are represented in terms of a rotation about a fixed axis as

$$\boldsymbol{q} = \widehat{\mathbf{n}} \sin\left(\frac{\phi}{2}\right) \in \mathbf{R}^3 \tag{3}$$

$$q_0 = \cos\left(\frac{\phi}{2}\right) \in \mathbf{R}, \tag{4}$$

where $\widehat{\mathbf{n}}$ and ϕ denote the Euler rotation axis and the rotation angle about this axis, respectively. We adopt the notation "$\otimes$" for quaternion multiplication defined by

$$\mathbf{q} \otimes \mathbf{p} = \begin{bmatrix} q_0\boldsymbol{p} + p_0\boldsymbol{q} + \boldsymbol{q} \times \boldsymbol{p} \\ q_0 p_0 - \boldsymbol{q}^T\boldsymbol{p} \end{bmatrix}, \tag{5}$$

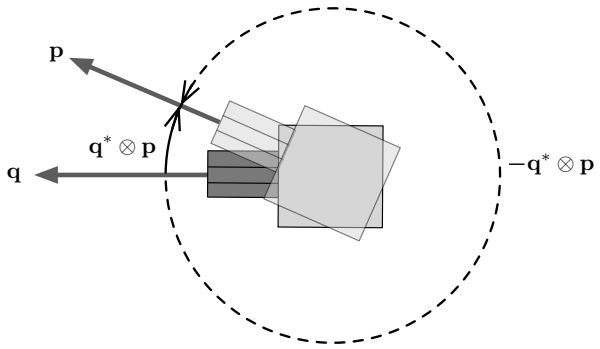

Figure 1. Attitude difference/error of p with respect to q and with respect to $-\mathrm{q}$. In this example, $\mathrm{q}^\star \otimes \mathrm{p}$ exhibits a geodesic rotation error over $-\mathrm{q}^\star \otimes \mathrm{p}$

where $\mathbf{q} = [\boldsymbol{q}^T \ q_0]^T$ and $\mathbf{p} = [\boldsymbol{p}^T, \ p_0]^T$. Another quaternion operation is the *quaternion transpose* defined as $\mathbf{q}^\star = [\,-\boldsymbol{q}^T \ q_0\,]^T$ which facilitates the judicious definition for attitude difference/error of $\mathbf{p}$ with respect to $\mathbf{q}$ via

$$\mathbf{q}_e := \mathbf{q}^\star \otimes \mathbf{p} = \begin{bmatrix} q_0\boldsymbol{p} - p_0\boldsymbol{q} - \boldsymbol{q} \times \boldsymbol{p} \\ q_0 p_0 + \boldsymbol{q}^T\boldsymbol{p} \end{bmatrix}, \tag{6}$$

where $\mathbf{q}$, $\mathbf{p}$ and $(\mathbf{q}^\star \otimes \mathbf{p}) \in S^3$. Note that the identity quaternion is signified by $\mathbf{q_I} = [\,0\ 0\ 0\ 1\,]^T$.

Given the attitude $\mathbf{q}$, the position vector $\boldsymbol{y}$ in body coordinates can be represented in the inertial coordinates as

$$\boldsymbol{y}' = \mathbf{q} \otimes \boldsymbol{y} \otimes \mathbf{q}^*, \tag{7}$$

where $\boldsymbol{y}'$ denotes the position vector expressed in the inertial coordinates. We note here that Eq. (7) is also interpreted as a rotation $\mathbf{q}$ of the vector $\boldsymbol{y}$.

Unit quaternion space S^3 doubly covers $\mathsf{SO}(3)$. This can be observed from the map $R : \mathbf{q} \in S^3 \to \mathsf{SO}(3)$ defined as

$$R(\mathbf{q}) = I_3 + 2q_0[\boldsymbol{q}]_\times + 2[\boldsymbol{q}]_\times^2, \tag{8}$$

where $[\boldsymbol{q}]_\times$ denotes the cross product operator in the matrix form associated with $\boldsymbol{q}$. Thus, we have

$$R(\mathbf{q}) = R(-\mathbf{q}). \tag{9}$$

This implies that the unit quaternion inherently possesses a sign ambiguity; when the error unit quaternion, Eq. (6) is considered, this ambiguity leads to having two choices–attitude error of $\mathbf{p}$ with respect to $\mathbf{q}$ and error of $\mathbf{p}$ with respect to $-\mathbf{q}$, where one exhibits a geodesic rotation error while the other a non-geodesic rotation error. See Fig. 1 for a graphical depiction of this observation. Note that in the continuous feedback control, this property combined with the existence of the extra unstable equilibrium of $-\mathbf{q}$, is referred to as the *unwinding phenomenon*.[18]

The key idea to avoid an undesired large angle rotation is to use a metric which can captures the geodesic distance in S^3 as a Euclidean distance between the current orientation and desired orientation. This is a straightforward result as the arc length (geodesic rotation) between two points on the unit sphere is proportional to the chord length between these points, as shown in the Fig.

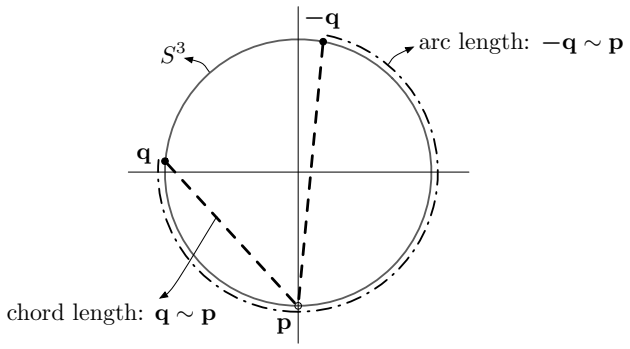

Figure 2. Chord length can be used to determine which arc length is geodesic. In this example, $\| \mathbf{p} - \mathbf{q} \|$ is shorter than $\| \mathbf{p} + \mathbf{q} \|$.

2. Therefore, given the current attitude $\mathbf{p}$ and the desired attitude $\mathbf{q}$, we update the desired attitude between $\mathbf{q}$ and $-\mathbf{q}$ depending on the choice that yields the smaller chord length, namely between

$$\| \mathbf{p} - \mathbf{q} \| \quad \text{and} \quad \| \mathbf{p} + \mathbf{q} \|. \tag{10}$$

In Fig. 2, we observe that $\mathbf{q}$ has a shorter distance from $\mathbf{p}$ on S^3 as compared with $-\mathbf{q}$. This chordal approach is subsequently used in our discussion on the optimal control for spacecraft reorientation. We note that the fact that unit quaternions can represent the attitude error in two distinct ways is not always disadvantage. This is in light of the fact that rotation matrices can not distinctly represent rotations $\theta < -\pi$ and $\theta \geq \pi$. For example, the rotation $\frac{3}{2}\pi$ represented by R is identical to the rotation $-\frac{1}{2}\pi$ about the same axis, i.e.,

$$R\Big(\frac{3}{2}\pi, \boldsymbol{n}\Big) = R\Big(-\frac{1}{2}\pi, \boldsymbol{n}\Big), \tag{11}$$

where $\boldsymbol{n}$ denotes a rotation axis. This can be important when the non-geodesic rotation is required for space science missions.

RIGID BODY DYNAMICS WITH REACTION WHEELS

In this section, we briefly review fundamentals of the dynamic equations for a spacecraft with reaction wheels. The kinematic equation between the spacecraft angular velocity and the unit quaternions is given by[19]

$$\dot{\mathbf{q}}(t) = \frac{1}{2}\mathbf{q}(t) \otimes \tilde{\boldsymbol{\omega}}(t), \tag{12}$$

where $\mathbf{q}(t)$ is the unit quaternion representing the attitude of the rigid body at time t, and $\boldsymbol{\omega}(t) \in \mathbf{R}^3$ denotes the angular velocity of the spacecraft in the body frame and $\tilde{\boldsymbol{\omega}}(t) = [\,\boldsymbol{\omega}^T \;\; 0\,]^T_{4\times 1}$. The attitude dynamics of the rigid spacecraft, equipped with three reaction wheels rotating along the spacecraft's principal axes, can be described as[21]

$$J\dot{\boldsymbol{\omega}}(t) = (J\boldsymbol{\omega} + J_r\boldsymbol{\omega}_r) \times \boldsymbol{\omega} - J_r\boldsymbol{u} \tag{13}$$

$$\dot{\boldsymbol{w}}_r = \boldsymbol{u} \tag{14}$$

where $J = \text{diag}(J_1,\ J_2,\ J_3)$ denotes the inertia matrix of the spacecraft in the body frame, $J_r = \text{diag}(J_{r1},\ J_{r2},\ J_{r3})$ denotes the inertia matrix of the spacecraft's reaction wheels in the body frame, and $\boldsymbol{u}(t) \in \mathbf{R}^3$ represents the control torque inputs on reaction wheels. The torque inputs

are restricted by current limitations on the electric motors and maximum angular velocities of the wheels. In this paper, we assume that all external disturbances and uncertainty on the spacecraft dynamics are negligible.

ATTITUDE CONSTRAINED ZONES

In this section, we define two types of attitude constrained zones that will be the focus of our discussion in this paper:

1. Attitude Forbidden Zone A set of spacecraft orientations, such as the set of attitudes that lead the sensitive on-board instruments to have a direct exposure to certain celestial objects, e.g., the sun, is considered as an attitude forbidden zone. Multiple constrained zones can be specified with respect to a single instrument boresight vector.

2. Attitude Mandatory Zone A set of spacecraft orientations, such as the set of attitudes that lead certain on-board instruments point toward specified objects, e.g., pointing a high gain antenna to a ground station, is considered as an attitude mandatory zone. The attitude mandatory zones for each instrument should be mutually feasible.

Suppose that an angle strictly greater than θ should be maintained between the normalized boresight vector $\boldsymbol{y}$ of the spacecraft instrument and the normalized vector $\boldsymbol{x}$ pointing toward a certain celestial object, as shown in Fig. 3. Note that $\boldsymbol{x}$ is given in the inertial coordinates when $\boldsymbol{y}$ is represented in body coordinates. Then, this requirement can be expressed as[16,17]

$$\boldsymbol{x} \cdot \boldsymbol{y}' < \cos\theta. \tag{15}$$

By Eq. (7), the vector $\boldsymbol{y}$ in body coordinates can be represented in the inertial coordinates as

$$\begin{aligned} \boldsymbol{y}' &= \mathbf{q} \otimes \boldsymbol{y} \otimes \mathbf{q}^* \\ &= \boldsymbol{y} - 2(\boldsymbol{q}^T\boldsymbol{q})\boldsymbol{y} + 2(\boldsymbol{q}^T\boldsymbol{y})\boldsymbol{q} - 2q_0(\boldsymbol{y}\times\boldsymbol{q}), \end{aligned} \tag{16}$$

where $\boldsymbol{y}$ now denotes the instrument's boresight vector represented in the inertial coordinates, taking into account the spacecraft attitude $\mathbf{q}$. Combining Eqs. (15), (16) yields

$$2\boldsymbol{q}^T\boldsymbol{y}\boldsymbol{q}^T\boldsymbol{x} - \boldsymbol{q}^T\boldsymbol{q}\boldsymbol{x}^T\boldsymbol{y} + q_0^2\boldsymbol{x}^T\boldsymbol{y} - 2q_0\boldsymbol{q}^T(\boldsymbol{x}\times\boldsymbol{y}) < \cos\theta. \tag{17}$$

After some algebraic manipulations, we thus obtain

$$\mathbf{q}^T \begin{bmatrix} A & b \\ b^T & d \end{bmatrix} \mathbf{q} < 0, \tag{18}$$

where

$$\begin{aligned} A &= \boldsymbol{x}\boldsymbol{y}^T + \boldsymbol{y}\boldsymbol{x}^T - (\boldsymbol{x}^T\boldsymbol{y} + \cos\theta)\,\mathbf{I}_3, \\ b &= -\boldsymbol{x}\times\boldsymbol{y}, \qquad d = \boldsymbol{x}^T\boldsymbol{y} - \cos\theta. \end{aligned} \tag{19}$$

Note that A, b, and d are constant. Such a representation, on the other hand, enables the parameterization of the two aforementioned constrained zones into the form of *quadratic inequalities*, as we proceed to include them in the optimal control problem.

Complement of Attitude Forbidden Zones

Let the unit quaternion $\mathbf{q} \in S^3$ describe the attitude of the spacecraft whose instrument boresight vector $\boldsymbol{y}$, e.g., a telescope, lies *outside of the attitude forbidden zone*, i.e., $\beta_2 > \theta_2$ in Fig. 3. Then the subset $\mathbf{Q}_{\boldsymbol{f_i}} \subseteq S^3$ satisfying the above condition can be represented as,

$$\mathbf{Q}_{\boldsymbol{f_i}} = \{\, \mathbf{q} \in S^3 \mid \mathbf{q}^T M_{f_i}(\theta_i)\mathbf{q} < 0\}, \tag{20}$$

with

$$M_{f_i}(\theta_i) = \begin{bmatrix} A_i & b_i \\ b_i^T & d_i \end{bmatrix}, \tag{21}$$

where

$$A_i = \boldsymbol{x}_i\boldsymbol{y}^T + \boldsymbol{y}\boldsymbol{x}_i^T - (\boldsymbol{x}_i^T\boldsymbol{y} + \cos\theta_i)\,\mathbf{I}_3, \tag{22}$$

$$b_i = -\boldsymbol{x}_i \times \boldsymbol{y}, \qquad d_i = \boldsymbol{x}_i^T\boldsymbol{y} - \cos\theta_i, \tag{23}$$

$$i = 1, 2, \ldots, n.$$

The index i represents the number of constrained objects associated with the on-board instrument. Thus M_{f_i} corresponds to the ith celestial object of the instrument. Moreover, $\boldsymbol{x}_i$ denotes the unit vector (specified in the inertial frame) for the ith constrained object to be avoided, while $\boldsymbol{y}$ indicates the unit vector (in the body frame) representing the boresight direction of the sensitive instrument on the spacecraft. The angle θ_i is the constraint angle about the direction of the ith object specified by $\boldsymbol{x}_i$ for the instrument boresight vector $\boldsymbol{y}$. Without loss of generality, the domain of the angle θ_i, for all i, is restricted to be $(0, \pi)$. We note that an attitude forbidden zone with $\theta_i \geq \frac{1}{2}\pi$ represents the same attitude constrained zone on the celestial sphere as *the attitude mandatory zone* with an angle $\pi - \theta_i$. The attitude forbidden zone is generally defined not only with respect to the number of onboard sensitive instruments m, but also with respect to the number of constraint objects n.

Attitude Mandatory Zone

The set $\mathbf{Q}_{\boldsymbol{m}} \subseteq S^3$ represents possible attitude of the spacecraft on which the boresight vector of an on-board instrument, e.g., an antenna, lies *inside the attitude mandatory zone*, i.e., $\beta_m < \theta_m$ in Fig. 4. This set can be represented as,

$$\mathbf{Q}_{\boldsymbol{m}} = \{\, \mathbf{q} \in S^3 \mid \mathbf{q}^T M_m(\theta_m)\mathbf{q} > 0\,\}, \tag{24}$$

where $M_m(\theta_m)$ and θ_m are defined analogous to Eq. (21), with respect to the boresight vector of an on-board instrument, which should stay in the attitude mandatory zone. The angle θ_M in Eq. (24) is the constraint angle for the attitude mandatory zone about the direction of the object specified by $\boldsymbol{x}_1$ in Fig. 3. Note that we have considered the case where only one attitude mandatory zone is present; this is without loss of generality, as if multiple mandatory zones are present, only the set defined by their intersection can be considered.

OPTIMAL ENERGY/TIME PROBLEM

In this section, we formulate the problem of reorienting a spacecraft with a dynamic model described in the previous section. We consider a rest-to-rest maneuver only. The optimal energy/time

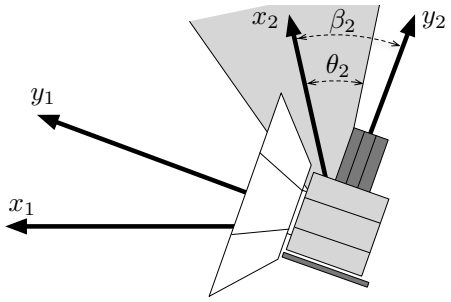

Figure 3. An attitude forbidden zone associated with an instrument boresight vector y_2.

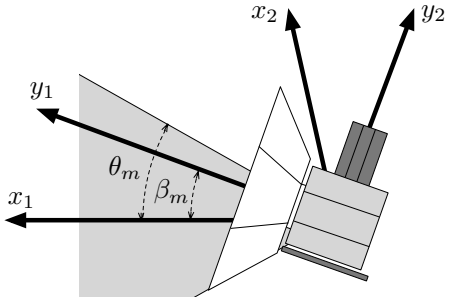

Figure 4. An attitude mandatory zone associated with an instrument boresight vector y_1.

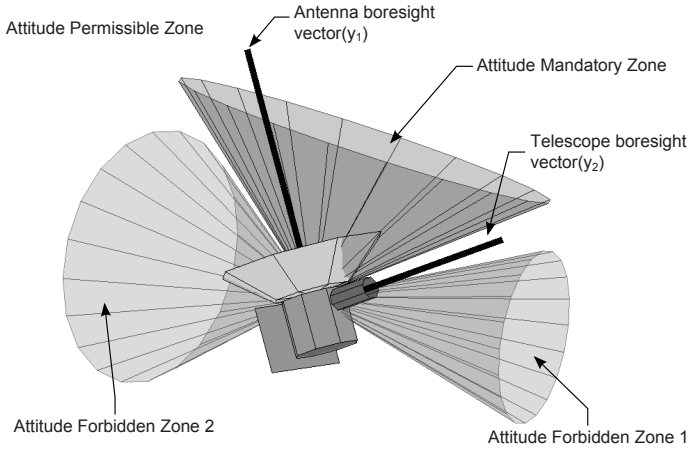

Figure 5. Two types of constrained zones shown on the celestial space. Attitude Mandatory zone is associated with an antenna boresight vector y_1 while a telescope boresight vector y_2 is associated with Attitude Forbidden zone 1 and 2.

spacecraft reorientation control problem in the presence of attitude constrained zones is then determined by finding the state $\mathbf{q} \in S^3$ and the control torques on reaction wheels $\boldsymbol{u} \in \mathbf{R}^3$ that minimize the performance cost

$$J = \int_{t_0}^{t_f} \big(\rho + (1-\rho)|\boldsymbol{u}(t)| \big) dt. \tag{25}$$

Note that ρ denotes a weighting factor on the time, where $\rho = 0$ and $\rho = 1$ yield the energy optimal and time optimal performance cost, respectively. This is subject to the differential dynamic constraints for $t \in [t_0,\, t_f]$,

$$\dot{\mathbf{q}}(t) = \frac{1}{2}\mathbf{q}(t) \otimes \tilde{\boldsymbol{\omega}}(t) \tag{12}$$

$$J\dot{\boldsymbol{\omega}}(t) = (J\boldsymbol{\omega} + J_r\boldsymbol{\omega}_r) \times \boldsymbol{\omega} - J_r\boldsymbol{u} \tag{13}$$

$$\dot{\boldsymbol{w}}_r = \boldsymbol{u}, \tag{14}$$

the boundary conditions

$$\mathbf{q}(t_0) = \mathbf{q}_{t_0}, \;\; \mathbf{q}(t_f) = \mathbf{q}_{t_f}, \;\; \boldsymbol{\omega}(t_0) = \mathbf{0}, \;\; \boldsymbol{\omega}(t_f) = \mathbf{0}, \quad \boldsymbol{\omega}_r(t_0) = \mathbf{0}, \tag{26}$$

control constraints, angular velocity limits on spacecraft and reaction wheels

$$|\, u_i \,| \leq \beta_u, \tag{27}$$

$$|\, \omega_i \,| \leq \beta_\omega, \tag{28}$$

$$|\, \omega_{r_i} \,| \leq \beta_{\omega_r}, \quad \text{for } i = 1, 2, 3 \tag{29}$$

path constraints for n attitude forbidden zones

$$\boldsymbol{q}^T M_{f_i} \boldsymbol{q} < 0, \quad \text{for } i = 1, ..., n \tag{30}$$

and path constraints for attitude mandatory zone

$$\boldsymbol{q}^T M_m \boldsymbol{q} > 0. \tag{31}$$

This optimal control problem was solved by a Gauss pseudospectral method (direct optimal control method) using the open source optimal control software GPOPS[15] in conjunction with the nonlinear programming problem solver SNOPT and the automatic differentiator INTLAB.

GAUSS PSEUDOSPECTRAL METHOD

Gauss pseudospectral method is a class of direct collocation methods where the optimal control problem is transcribed into a nonlinear programming problem (NLP) by approximating the state and control states using global orthogonal polynomials and collocating the differential dynamic equations on *Legendre-Gauss* collocation points. The time interval $t \in [t_0,\, t_f]$ can be normalized to the time interval $\tau \in [-1,\, 1]$ via the affine transformation,

$$\tau = \frac{2t - t_f - t_0}{t_f - t_0}. \tag{32}$$

The states $\mathbf{q}(\tau)$ is approximated by the polynomial $\tilde{\mathbf{q}}(\tau)$ using a basis of $N+1$ Lagrange interpolating polynomials on the time interval of $[-1,\ 1]$ as

$$\mathbf{q}(\tau) \approx \tilde{\mathbf{q}}(\tau) = \sum_{i=0}^{N} \mathbf{q}(\tau_i) L_i(\tau_i), \tag{33}$$

where $L_i(\tau)$ is the ith Lagrange polynomial defined as

$$L_i(\tau) = \prod_{j=0, j\neq i}^{N} \frac{\tau - \tau_j}{\tau_i - \tau_j}, \quad (i = 0, ..., N). \tag{34}$$

The derivative of the state approximation is similarly obtained as

$$\dot{\mathbf{q}}(\tau_k) \approx \dot{\tilde{\mathbf{q}}}(\tau_k) = \sum_{i=0}^{N} \tilde{\mathbf{q}}(\tau_i) \dot{L}_i(\tau_k) = \sum_{i=0}^{N} D_{k,i} \tilde{\mathbf{q}}(\tau_i), \tag{35}$$

where $D_{k,i}$ are element of non-square matrix $D \in \mathbf{R}^{N\times(N+1)}$ called *Gauss pseudospectral differentiation matrix*. See ref.[22,23] for more details. The performance cost in terms of τ is approximated using a Gauss quadrature as

$$J = \frac{t_f - t_0}{2} \sum_{k=1}^{N} w_k \big(\rho + (1-\rho) |\, \boldsymbol{u}(\tau_k)\, |\big), \tag{36}$$

where w_k are the Gauss weights. The above performance index together with approximated constraints by Eqs. (33) and (33) lead to formulation of a nonlinear programming with the initial and final states $\mathbf{q}(t_0) = \tilde{\mathbf{q}}(\tau_0)$ and $\mathbf{q}(t_f) = \tilde{\mathbf{q}}(\tau_f)$, respectively, which can be solved using SNOPT nonlinear solver.

NUMERICAL RESULTS

In this section, for two scenarios we present several numerical results including energy optimal and time optimal missions. The first scenario is assumed to have four attitude forbidden zones while the second scenario is assumed to have three attitude forbidden zones and one mandatory zone.

Scenario 1 (four attitude forbidden zones)

We consider a scenario in which the spacecraft is re-targeting its telescope while minimizing energy/time consumption and avoiding *four attitude forbidden zones* in the spacecraft rotational configuration space. The four attitude forbidden zones are randomly chosen, not overlapping with each other. Both initial and desired attitudes are randomly chosen in the *complement of attitude forbidden zones*, not violating the constrained zones as

$$\mathbf{q}_{t_0}^T M_{f_i} \mathbf{q}_{t_0} < 0 \quad \text{and} \quad \mathbf{q}_{t_f}^T M_{f_i} \mathbf{q}_{t_f} < 0, \quad i = 1, 2, 3, 4, \tag{37}$$

where $\mathbf{q}_{t_0}$ and $\mathbf{q}_{t_f}$ are the initial and desired unit quaternions, respectively. It has been assumed that the spacecraft carries a light-sensitive instrument with a fixed boresight in the spacecraft body axes, directed along the Z direction. Simulation parameters are are given in Table 1. Figs. 6-7 trace the geodesic pointing direction of the light-sensitive instrument on the celestial sphere as

Table 1. Case 1 simulation parameters

J	diag [54, 63, 59] $kg \cdot m^2$		
J_r	diag [1, 0.8, 0.8] $kg \cdot m^2$		
$\|\omega\|$	$\leq$ 0.3 rad/s		
$\|\omega_r\|$	$\leq$ 6 rad/s		
$\|u\|$	$\leq$ 2 rad/s^2		
t_f	$\leq 20s$		
Initial Attitude $\mathbf{q}_{t_0}$	[0.6085, -0.6300, -0.2369, -0.4204]		
Desired Attitude $\mathbf{q}_{t_f}$	[-0.0238, 0.7127, -0.2734, -0.6455]		
constrained object 1	[0.1632, -0.9863, 0.0250]	40 deg	Forbidden
constrained object 2	[0.0734, 0.6938, 0.7164],	40 deg	Forbidden
constrained object 3	[-0.5000, 0.6634, -0.5567],	30 deg	Forbidden
constrained object 4	[-0.0677, -0.4628, -0.8839]	20 deg	Forbidden

well as the same trajectory on the 2D cylindrical projection of the celestial sphere for the time and energy optimal case; on the other hand, Figs. 8-9 depict the non-geodesic rotations for the time and energy optimal case. The initial attitude is denoted by '$\circ$' and the desired attitude is denoted by '$\times$'. Figs. 10-13 exhibit the unit quaternions, angular velocities, control inputs and reaction wheel angular velocities over time. Note that the time optimal case terminates in about 14 seconds while the energy optimal case in 20 seconds.

Scenario 2 (three attitude forbidden zones and one attitude mandatory zone)

In scenario 2, we examine a more complex reorientation maneuver keeping a fixed antenna boresight vector within a certain angle for continuous communication with the ground station while the spacecraft is re-targeting its light sensitive instrument avoiding multiple bright objects or constrained zones. For this scenario, the antenna has been aligned along the Z-axis while the sensitive instrument has been aligned along the Y-axis; We note that since this case includes a attitude mandatory zone as well as attitude forbidden zones, selecting the *right signed* unit quaternion for geodesic rotation plays a more crucial role than for the first case; the non-geodesic rotation may not be able to reach the final orientation. The three attitude forbidden zones are randomly chosen, not overlapping with each other and both initial and desired attitudes are chosen not violating the *complement of attitude forbidden zones* and *attitude mandatory zone* as

$$\mathbf{q}_{t_0}^T M_{f_i} \mathbf{q}_{t_0} < 0 \text{ and } \mathbf{q}_{t_f}^T M_{f_i} \mathbf{q}_{t_f} < 0, \quad i = 1, 2, 3, \tag{38}$$

and

$$\mathbf{q}_{\boldsymbol{t_0}}^T M_m \mathbf{q}_{\boldsymbol{t_0}}^T > 0 \text{ and } \mathbf{q}_{\boldsymbol{t_f}}^T M_m \mathbf{q}_{\boldsymbol{t_f}}^T > 0. \tag{39}$$

Table 2. Case 2 simulation parameters

J	diag [54, 63, 59] $kg \cdot m^2$		
J_r	diag [1, 0.8, 0.8] $kg \cdot m^2$		
$\|\omega\|$	$\leq$ 0.3 rad/s		
$\|\omega_r\|$	$\leq$ 6 rad/s		
$\|u\|$	$\leq$ 2 rad/s^2		
t_f	$\leq 20s$		
Initial Attitude	[0.7143, 0.6365, -0.1300, 0.2602]		
Desired Attitude	[0.2297, -0.0081, -0.4909, 0.8404]		
constrained object 1	[-0.8138, 0.5483, -0.1926]	70 deg	Mandatory
constrained object 2	[0, -1, 0],	40 deg	Forbidden
constrained object 3	[0, 0.8192, 0.5736],	30 deg	Forbidden
constrained object 4	[-0.1220, -0.1397, -0.9827]	20 deg	Forbidden

Note that the set of physically feasible conditions is a subset in the configuration space that satisfies the above requirements. Figs. 14 and 15 demonstrate reorientation maneuvers while keeping the antenna's boresight vector within 70 degrees of the mandatory cone (black shaded area). The simulation parameters for this scenario are given in Table 2. Figs. 16-19 show the time histories for the quaternions, angular velocities, control inputs, and the reaction wheel angular velocities.

CONCLUSIONS

In this paper, quaternion-based energy and time optimal spacecraft reorientations in the presence of complex attitude constrained zones have been examined. This has been achieved via a Gauss pseudospectral method that utilizes the quaternion attitude constrained zone parametrization. Ambiguity on geodesic/non-geodesic rotations has been discussed and a novel algorithm is presented. Extensive simulation results have been presented within two distinct scenarios to demonstrate the viability of the proposed methodology.

REFERENCES

[1] C. R. McInnes, "Large angle slew maneuvers with autonomous sun vector avoidance," *AIAA Journal of Guidance, Control and Dynamics*, vol. 17, no. 4, pp. 875-877, 1994.

[2] S.R. Stadin, and R.W. Davis, "The Small Satellite Revolution-Back to the Future," IAF-93-U, 1993.

[3] E. D. Jin, and Z. W. Sun, "Robust attitude tracking control of flexible spacecraft for achieving globally asymptotic stability," *International Journal of Robust and Nonlinear Control,* vol. 19, pp. 1201-1223, 2009.

[4] M. Xin, and H. Pan, "Indirect Robust Control of Spacecraft via Optimal Control Solution," *IEEE Transactions on Aerospace and Electronic Systems,* vol.48, no.2, pp. 1798-1809, 2012.

[5] W.M. Haddad, V. S. Chellaboina, J. L. Fausz, and A. Leonessa, "Optimal nonlinear robust control for nonlinear uncertain cascade systems," *Proceedings of the American Control Conference,* June 1997.

[6] U. Lee and M. Mesbahi, "Spacecraft reorientation in presence of attitude constraints via logarithmic barrier potentials" *Proceedings of the American Control Conference,* pp. 450-455, 2010.

[7] G. Ma, Y. Zhuang, C. Li, and H. Huang, "Pseudospectral Method for Optimal Motion Planning of a Rigid Underactuated Spacecraft," *2010 8th IEEE International Conference on Control and Automation*, Xianmen, China, 2010.

[8] K. Spindler, "New methods in on-board attitude control," *Advanced in the Astronautical Sciences*, vol. 100, no. 2, pp. 111-124, 1998.

[9] H. B. Hablani, "Attitude commands avoiding bright objects and maintaining communication with ground station," *Journal of Guidance, Control, and Dynamics*, vol. 22, no. 6, pp. 759-767, 1999.

[10] E. Frazzoli, M. A. Dahleh, E. Feron, and R. P. Kornfeld, "A randomized attitude slew planning algorithm for autonomous spacecraft," *Proceedings of the AAIA Guidance, Navigation, and Control Conference*, 2001.

[11] R. P. Kornfeld, "On-board autonomous attitude maneuver planning for planetary spacecraft using genetic algorithms," *Proceedings of the AIAA Conference on Guidance, Navigation and Control*, 2003.

[12] P. Cui, W. Zhong, and H. Cui, "Onboard spacecraft slew-planning by heuristic state-space search and optimization," *International Conference on Mechatronics and Automation*, pp. 2115-2119, 2007.

[13] S. N. Singh and W. Yim, "Nonlinear adaptive backstepping design for spacecraft attitude control using solar radiation pressure," *Proceedings of the 41th IEEE Conference on Decision and Control*, Las Vegas, Nevada, 2002.

[14] R. Kristiansen, and P. J. Nicklasson, "Satellite attitude control by quaternion-based backstepping", *Proceedings of American Control Conference*, Portland, Oregon, USA 2005.

[15] A. V. Rao, D. A. Benson, C. Darby, M. A. Patterson, C. Francolin, I. Sanders, and G. T. Huntington, "Algorithm 902: GPOPS, A MATLAB software for solving multiple-phase optimal control problems using the gauss pseudospectral method," *ACM Transaction on Mathematical Software,* vol 37, no. 2, Article 22, 2010.

[16] A. Ahmed, J. Alexander, D. Boussalis, W. Breckenridge, G. Macala, M. Mesbahi, M. San Martin, G. Singh, and E. Wong, *Cassini Control Analysis Book*, Jet Propulsion Laboratory, 1998.

[17] G. Singh, G. Macala, E. Wong, and R. Rasmussen, "A constraint monitor algorithm for the Cassini spacecraft," *Proceedings of the AIAA Guidance, Navigation, and Control Conference,* pp. 272-282, AIAA, Reston, VA, 1997.

[18] S. Bhat, and D. S. Bernstein, "A topological obstruction to continuous global stabilization of rotational motion and the unwinding phenomenon," *Systems & Control Letters*, vol. 39, no. 1, 63-70, 2000.

[19] B. Wie and P. Barba, "Quaternion feedback for spacecraft large angle maneuvers," *Journal of Guidance Control Dynamics,* vol. 8, no. 3, pp. 360-365, 1985.

[20] P. Singla, K. Subbarao, and J. Junkins, "Adaptive output feedback control for spacecraft rendezvous and docking under measurement uncertainty.", *Journal of Guidance, Control and Dynamics,* vol. 29, no. 4, pp. 892-902, 2006.

[21] A. Tewari, *Atmospheric and Space Flight Dynamics*, Birkhäuser, 2007.

[22] D. Garg, M. A. Patterson, W. W. Hager, A. V. Rao, D. A. Benson and G. T. Huntington, "A Unified Framework for the Numerical Solution of Optimal Control Problems Using Pseudospectral Methods," *Automatica,* vol. 46, No. 11, 2010, pp. 1943-1851.

[23] D. Garg, M. A. Patterson, W. W. Hager, A. V. Rao, D. A. Benson and G. T. Huntington, "An Overview of Three Pseudospectral Method for the Numerical Solution of Optimal Control Problems.", *Advances in the Astronautical Sciences,* Univelt Inc., San Diego, 2010, pp. 475-487.

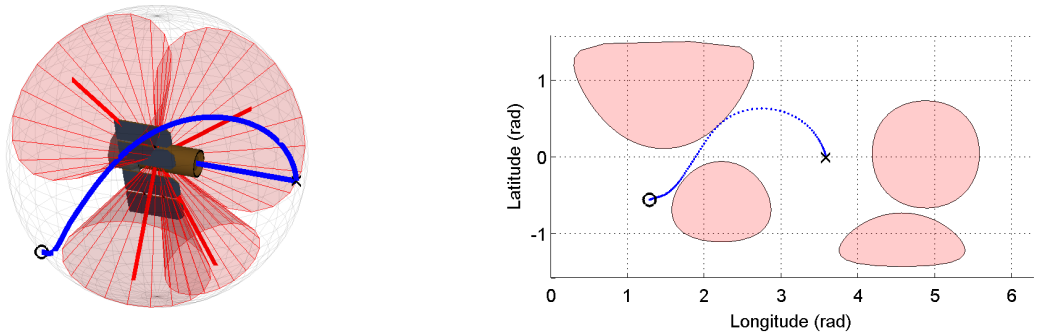

Figure 6. Geodesic/Time optimal: the traces of the telescope pointing direction on the celestial sphere and 2D cylindrical projection. The circle and the cross indicate the directions of the initial and final orientations, respectively.

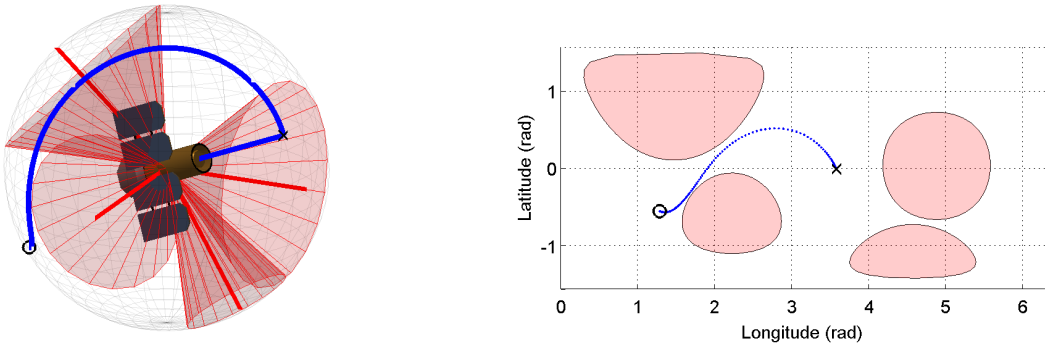

Figure 7. Geodesic/Energy optimal: the traces of the telescope pointing direction.

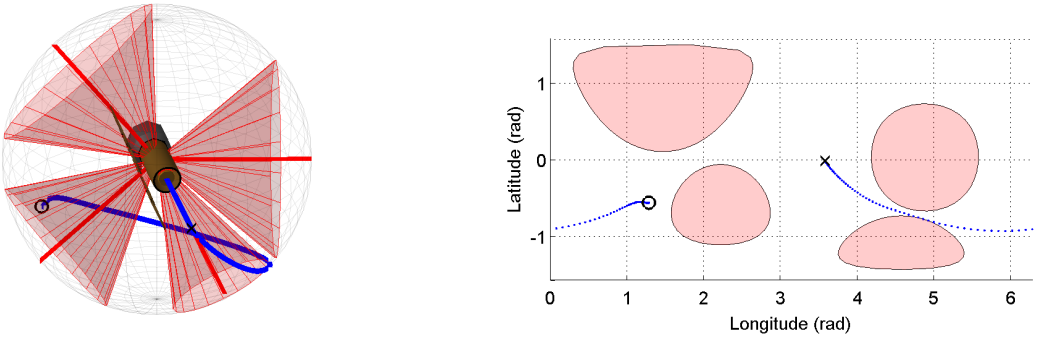

Figure 8. Non-geodesic/Time optimal: the traces of the telescope pointing direction.

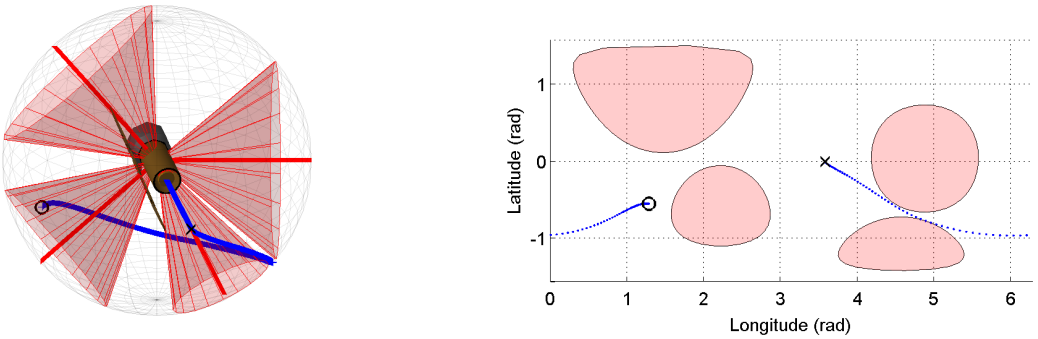

Figure 9. Non-geodesic/Energy optimal: the traces of the telescope pointing direction.

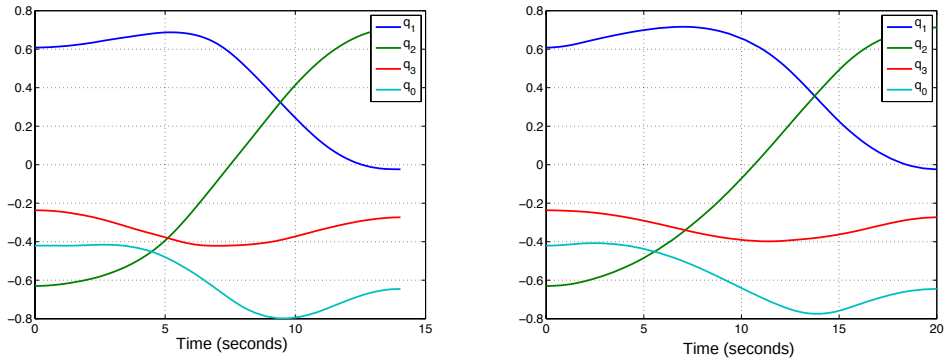

Figure 10. Quaternion trajectories for time optimal (left) and energy optimal case (right).

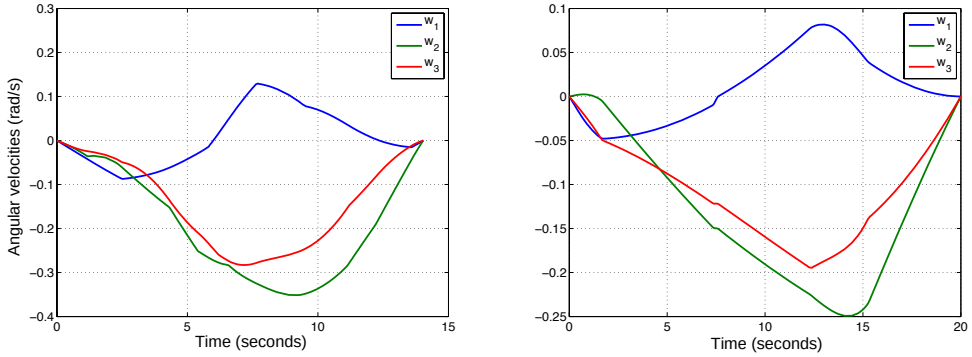

Figure 11. Spacecraft angular velocity trajectories for time optimal (left) and energy optimal case (right).

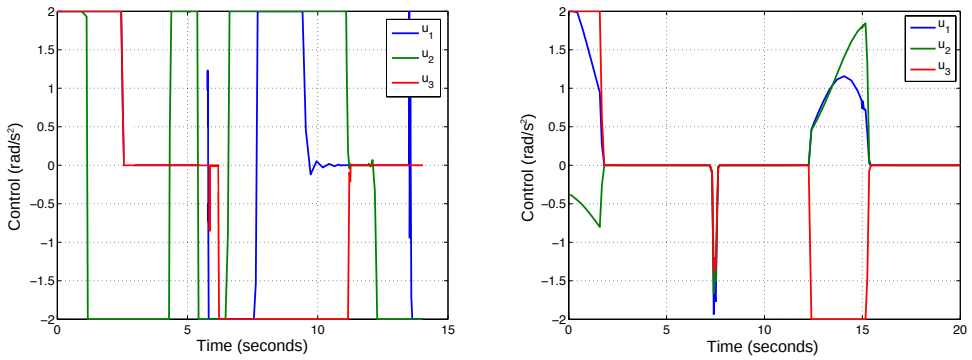

Figure 12. Control trajectories for time optimal (left) and energy optimal case (right).

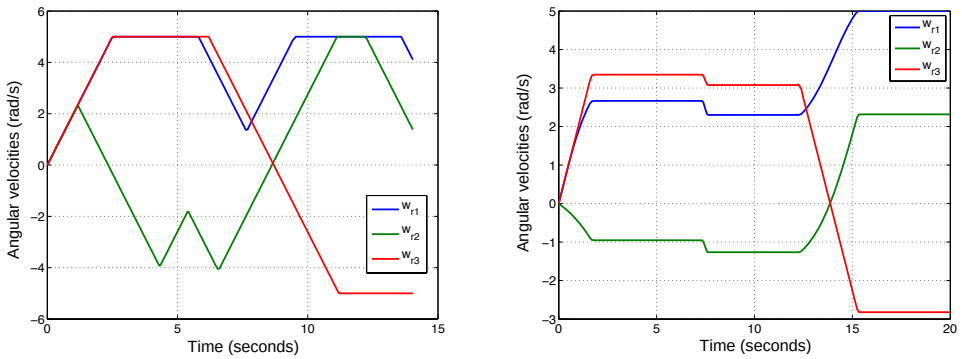

Figure 13. Reaction wheel angular velocitiy trajectories for time optimal (left) and energy optimal case (right).

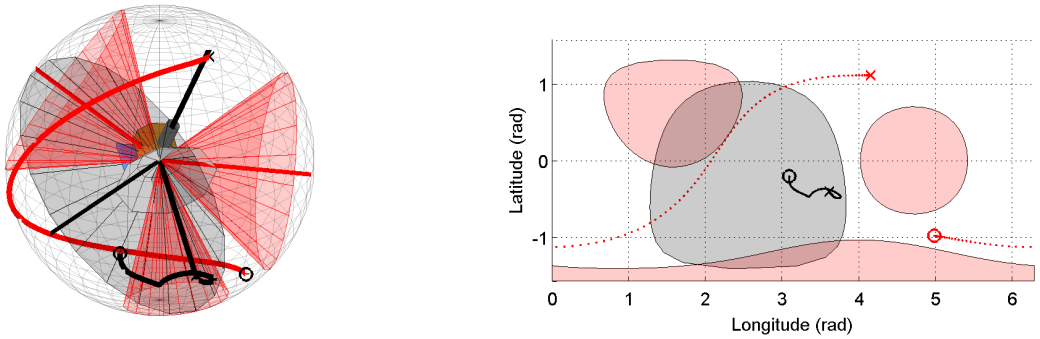

Figure 14. Geodesic/Time optimal: the traces of the telescope pointing vector and antenna boresight vector on the celestial sphere and 2D cylindrical projection in the presence of three attitude forbidden zones and one mandatory zone. The circle and the cross indicate the directions of the initial and final orientations, respectively.

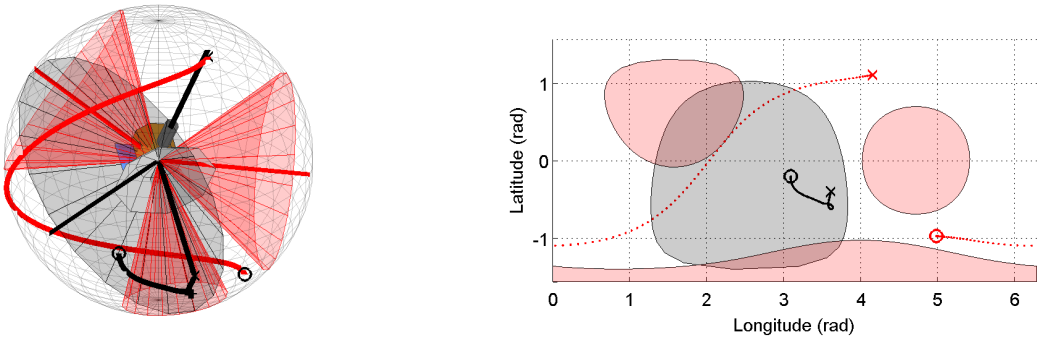

Figure 15. Geodesic/Energy optimal: the traces of the telescope pointing vector and antenna boresight vector.

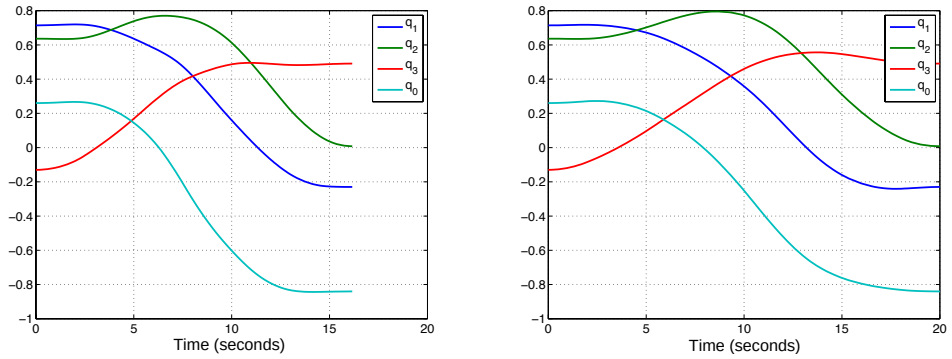

Figure 16. Uunit quaternion trajectories for time optimal (left) and energy optimal case (right).

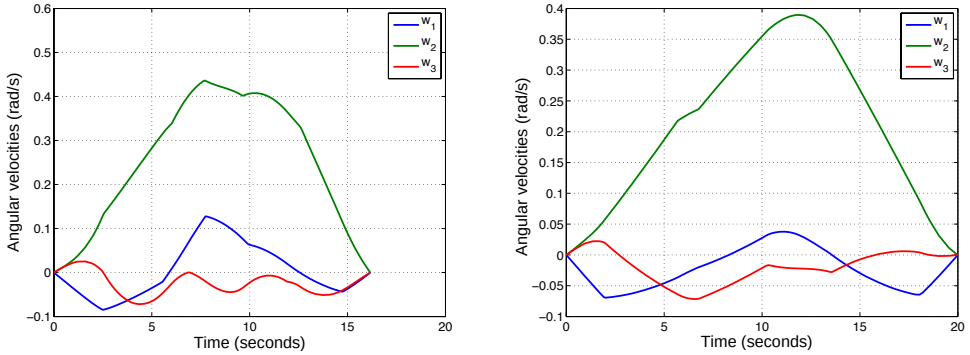

Figure 17. Spacecraft angular velocity trajectories for time optimal (left) and energy optimal case (right).

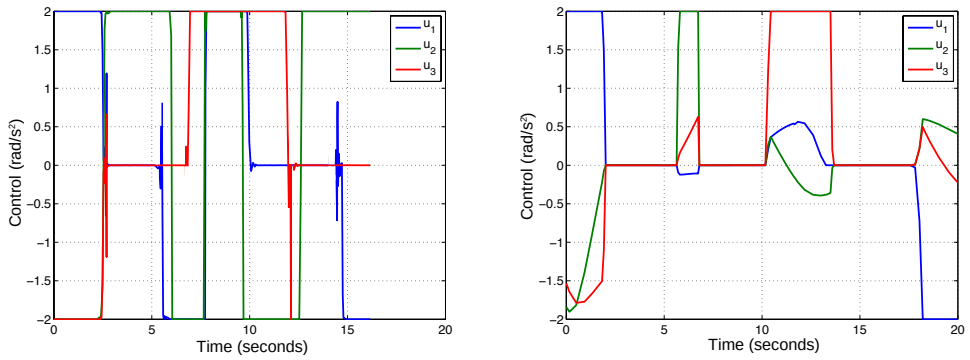

Figure 18. Control trajectories for time optimal (left) and energy optimal case (right).

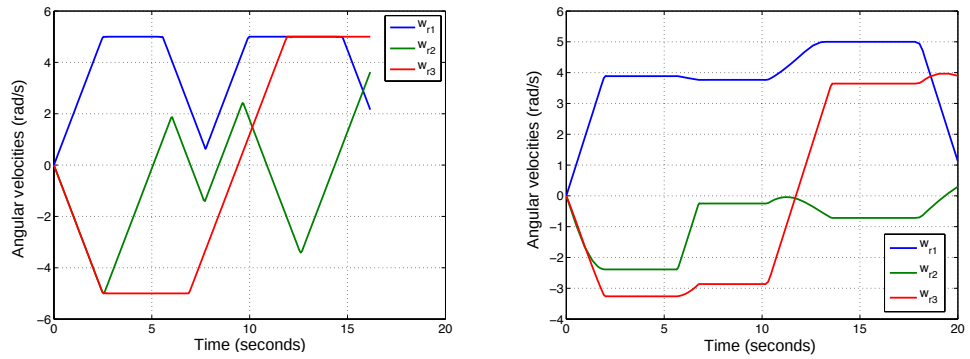

Figure 19. Reaction wheel angular velocitiy trajectories for time optimal (left) and energy optimal case (right).